DYNAMIC STABILITY OF A BEARINGLESS CIRCULATION CONTROL ROTOR BLADE IN HOVER

Inderjit Chopra
Center for Rotorcraft Education and Research
Department of Aerospace Engineering
University of Maryland
College Park, MD 20742

Abstract

The aeroelastic stability of flap bending, lead-lag bending and torsion of a bearingless circulation control rotor blade in hover is investigated using a finite element formulation based on Hamilton's principle. The flexbeam, the torque tube and the outboard blade are discretized into beam elements, each with fifteen nodal degrees of freedom. Quasisteady strip theory is used to evaluate the aerodynamic forces and the airfoil characteristics are represented either in the form of simple analytical expressions or in the form of data tables. The unsteady aerodynamic effects are introduced approximately through dynamic wake induced inflow modeling. The nonlinear equations of motion are solved for steady blade deflections using an iterative procedure. The flutter solution is calculated assuming blade motion to be a small perturbation about the steady solution, and the normal mode equations are used to reduce the number of equations. A correlation study of analytical results with the experimental data is attempted for selected bearingless blade configurations with conventional airfoil characteristics. Then stability results are obtained for circulation control bearingless configurations consisting of a single flexbeam with a wrap-around type torque tube and the pitch links located at both the leading edge and the trailing edge of the torque tube. The stability is examined at various thrust levels and collective pitch settings.

NOMENCLATURE

a_r	reference lift curve slope (5.7/rad)
c	blade chord, m
c_d	blade section drag coefficient
c_ℓ	blade section lift coefficient
$c_{m_{.5}}$	blade section moment coefficient about midchord
C_T	rotor thrust coefficient $\frac{T}{\rho(\Omega R)^2 \pi R^2}$
C_μ	blowing momentum coefficient $\frac{\dot{m}V_j}{1/2\rho V^2 c}$
d	pitch link location from torque tube center, m
D	blade section drag force, N
e_d	aerodynamic center offset from elastic axis, positive aft, m
e_g	center of mass offset from elastic axis, positive forward, m
I_b	blade mass moment of inertia about flap axis, N-m-sec^2
L	blade section lift force, N
L_u, L_v, L_w	aerodynamic force per unit length in u,v,w, directions, N/m
m	mass per unit length of blade, N-sec^2/m^2
m_o	reference mass per unit length, N-sec^2/m^2
$M_{.5}$	blade section aerodynamic moment about midchord, N-m
M_ϕ	aerodynamic moment per unit length about elastic axis, N
n	number of elements
s	constant defining blowing distribution
R	rotor radius, m
t	time, sec
$u,v,w,$	elastic displacements in the x,y,z directions respectively, m
u_p	blade section normal velocity, m/sec
u_T	blade section inplane velocity, m/sec
V	blade section resultant air velocity, m/sec
v_i	induced inflow, m/sec
V_j	jet velocity (blowing), m/sec
w_p	pitch link displacement, m
$x,y,z,$	undeformed blade coordinates, m

Presented at the Second Decennial Specialists' Meeting on Rotorcraft Dynamics at Ames Research Center, Moffett Field, CA, November 7-9, 1984.

a	blade section angle of attack, rad
β_p	blade precone angle, rad
γ	Lock number $\rho a_r c R^4/I_b$
ρ	air density, N-sec^2/m^4
$\delta T, \delta V$	variation of kinetic and strain energies respectively
δW	virtual work done due to aerodynamic loads
θ	blade pretwist, rad
λ	rotor induced inflow ratio, $v_i/\Omega R$
ξ, η, ζ	deformed blade coordinates nondimensionalized wrt R
σ	solidity ratio, blade area/disk area
ϕ	elastic twist about elastic axis, rad
$\$$	geometric apparent twist about deflected elastic axis, due to coordinate transformations, rad
ψ	dimensionless time, Ωt
$\omega_v, \omega_w, \omega_\phi$	fundamental coupled rotating lead-lag, flap and torsion natural frequencies respectively
Ω	rotor blade angular speed, rad/sec
ζ	ratio of modal damping to critical damping
η_t	torque tube center offset from elastic axis, positive forward, m
η_f	flexbeam center offset from elastic axis, positive forward, m

Introduction

A circulation control rotor (CCR) utilizes circulation control (CC) aerodynamics for main rotor blade design. A CC airfoil is typically of quasi-elliptic profile with rounded trailing edge, and a thin jet of air is blown from a spanwise slot (Fig. 1). The air jet remains attached over the curved profile because of Coanda effect (balance of centrifugal force and suction pressure). In a CCR, the thrust vector can be controlled by modulation of blowing as well as geometric pitch. With a CCR, a high thrust is possible at reduced tip speeds and also the hub design can be simplified because of elimination of cyclic pitch. The application of CC technology is currently being evaluated in the design development of a full-scale rotor. One concern is the influence of blowing on the dynamics of the rotor blade.

With the availability of improved materials, recent rotor design trends are leaning towards hingeless blade configurations. A bearingless rotor is one such example where flap and lag hinges as well as pitch bearing are eliminated, and these are replaced by a root flexure consisting of flexbeam(s) and a torque tube (Fig. 2). The torsionally soft flexbeam(s) extends from the hub to about 15-40% of blade radius where it is connected to the main blade. The pitch control to the blade is applied through the torsionally stiff torque tube by rotating it with the pitch link which elastically twists the flexbeam(s). This results in a multiple-load-path structure because of the redundancy of load paths at the flexure. This causes however a more involved dynamic analysis.

The objective of the present paper is to examine aeroelastic stability of flap bending, lead-lag bending and torsion of a circulation control bearingless blade in hover.

A general review on aeroelastic stability of a rotating blade with conventional aerodynamics is given in References 1-2. Chopra and Johnson[3] formulated and analyzed the flap-lag-torsion aeroelastic stability of a CCR blade in hovering flight. Three degrees of motion were considered: rigid flap, lag and feather rotations about hinges at the blade root. The CC airfoil characteristics were represented in the form of simple analytical expressions. It was shown that the trailing edge blowing can have a major influence on blade aeroelastic stability. Recently Chopra[4] analyzed the aeroelastic stability of flap bending, lead-lag bending, and torsion of a CCR blade in hover using a finite element formulation. The CC airfoil characteristics in the form of data tables were used. Results were presented for several hingeless blade configurations. Again, it was shown that the blowing has an important influence on blade dynamics which must be considered in rotor design.

Sivaneri and Chopra[5] applied a finite element formulation to analyze the dynamics of a bearingless rotor blade in hover with conventional aerodynamic characteristics. Each of the flexbeams and the torque tube were modelled as individual elastic beams. The displacement compatibility conditions at the clevis, between the inboard flexure beams and the outboard blade, were satisfied. Results were also calculated using a simple equivalent-beam modelling wherein a bearingless blade is represented as a single beam with equivalent properties. Comparison of the two sets of results showed that the equivalent-beam modelling can be quite erroneous for some cases.

In the present paper, the above finite element formulation is modified to study the aeroelastic stability of a bearingless CCR blade in hover. The multibeams of the flexure, and the outboard blade idealized as an elastic beam, are all discretized into beam elements, each element with fifteen nodal degrees of freedom. There is a continuity of axial displacement u, flap bending w and w', lead-lag bending v and v' and geometric twist $\$$ between elements. Quasisteady strip theory is used to evaluate aerodynamic forces. The airfoil

characteristics are represented in the form of data tables. The influence of unsteady aerodynamics is introduced by using dynamic inflow modelling. The formulation is made quite general for nonuniform blades keeping in view the application to different types of bearingless configurations. First, a correlation study of analytical results with the experimental data is attempted for selected bearingless configurations with conventional airfoil characteristics. Then, stability resulty are obtained for circulation control bearingless configurations.

Formulation

The formulation details can be seen in References 4-5. The blade is treated as an elastic beam and undergoes axial displacement u, lead-lag bending displacement v, flap bending displacement w and elastic twist ϕ about a deformed elastic axis. Fig. 3 shows the deformed as well as undeformed blade positions. The rectangular coordinate system x,y,z is attached to the undeformed blade, wherein the x-axis coincides with the elastic axis. A point P on the undeformed elastic axis undergoes displacements u, v, w in the x,y,z directions respectively and occupies the position P' on the deformed elastic axis. Then the blade section containing point P' undergoes a rotation θ_1 about deformed elastic axis.

$$\theta_1 = \theta + \phi \qquad (1a)$$

and

$$\phi = \phi - \int_0^x v''w'dx \qquad (1b)$$

where θ is pretwist, ϕ is the geometric twist with respect to the undeformed axis (compatible with u,v,w) and ϕ is the elastic twist about the deformed elastic axis ξ. The formulation is based on Hamilton's principle

$$\int_{t_1}^{t_2}(\delta U - \delta T - \delta W)\, dt = 0 \qquad (2)$$

where δU, δT and δW are respectively the variation of strain energy, the variation of kinetic energy and the virtual work done. These energy expressions are made independent of the time derivatives of virtual displacements, δu, δv, δw and $\delta\phi$ and hence Eq. (2) can be written as

$$\delta U - \delta T - \delta W = 0 \qquad (3)$$

The aerodynamic forces are obtained using quasisteady strip-theory approximation. Forces of non-circulatory origin are also included. The section lift, drag and moment about the mid-chord (per unit span) are

$$L = \frac{1}{2}\rho V^2 c\, C_\ell(\alpha, C_\mu)$$

$$D = \frac{1}{20}\rho V^2 c\, C_d(\alpha, C_\mu) \qquad (4)$$

$$M_{.5} = \frac{1}{2}\rho V^2 c^2 C_{m_{.5}}(\alpha, C_\mu)$$

The aerodynamic coefficients C_ℓ, C_d and $C_{m_{.5}}$ are taken from data tables, and the numerical values for these coefficients are given at small steps: $\Delta\alpha$ of $1/2°$ and ΔC_μ of 1/200. The C_μ is blowing momentum coefficient defined as

$$C_\mu = \frac{\dot{m}V_j}{1/2\rho V^2 c} \qquad (5)$$

where $\dot{m}V_j$ is the jet momentum, $1/2\rho V^2$ is the dynamic pressure, and c is the blade chord.

The wake induced inflow is assumed uniform along the length of the blade and the steady component is calculated from the momentum theory

$$\lambda_0 = K_h(C_T/2)^{1/2} \qquad (6)$$

where K_h is an empirical factor and is assumed to be 1.15 and C_T is the steady thrust coefficient. With blade vibratory motion, unsteady flow environments are created and which will naturally result in dynamic induced inflow condition. For hover, a simple dynamic inflow model is used

$$\tau\dot{\lambda} + \lambda = \frac{K_h^2}{4\lambda_0} \qquad (7)$$

where τ is the time lag in arc radian and can be approximately taken as $.85/\lambda_0$. The λ is a time induced inflow component, a perturbation about the steady component λ_0. The ΔC_T is the perturbation thrust component caused by blade motions. The blowing momentum coefficient C_μ is not uniform along the length of the blade, and a general distribution is used for the formulation

$$C_\mu = C_{\mu_T}/\xi^s \qquad (8)$$

where s is a constant, $\xi = r/R$ and C_{μ_T} is blowing coefficient at blade tip. For simplicity of analysis, it is assumed that the blowing coefficient is constant within each element (based on midpoint of element).

Finite Element Discretization

The finite element formulation is based on energy principles (Hamilton). The flexbeam(s), the torque tube and the main outboard blade are all discretized into a number of beam elements. Each element (Fig. 4) consists of fifteen degrees of freedom. There is a continuity of u, v, v', w, w' and ϕ between elements, and there are three internal nodes, two for u and one for ϕ. The distribution for deflections over an element are represented in terms of element degrees of freedom and shape functions; a second order polynomial for ϕ and cubic polynomials for u, v and w.

Hamilton's principle in discretized form for n elements is expressed as

$$\sum_{i=1}^{n}(\delta U_i - \delta T_i - \delta W_i) = 0 \qquad (9)$$

where δU_i, δT_i and δW_i are virtual energy contributions from i^{th} element. During the assembly of element matrices, one has to use the displacement compatibility conditions at interelement boundaries to form global matrices. A simple analytical model of bearingless blade is shown in Fig. 5. The displacement compatability at the clevis is

$$\begin{aligned} u_t &= u_f = u_b \\ v_t &= v_f = v_b \\ v_t' &= v_f' = v_b' \\ w_t - \eta_t \phi_t &= w_f - \eta_f \phi_f = w_b \\ w_t' &= w_f' = w_b' \\ \phi_t &= \phi_f = \phi_b \end{aligned} \qquad (10)$$

where subscripts t, f and b respectively represent torque tube, flexbeam and b'ade.

Fig. 6 shows the root end of the torque tube with the control actuator located at the leading edge. The blade pitch is changed through the up and down movement of pitch link. The torque tube typically is very stiff torsionally as compared to the flexbeam. Therefore any vertical movement of the pitch link results in nearly rigid body pitch for the torque tube and an elastic twist distribution for the flexbeam. To obtain different blade pitch angles, one has to adjust the vertical position of pitch link, W_p. The pitch link flexibility is represented by spring stiffness K_p. Because of the pitch link flexibility, there will be an extra strain energy contribution for the last element of the torque tube, say V_p.

$$V_p = \frac{1}{2} K_p [w_1 + \phi_1 (d + \eta_t) - w_p]^2 \qquad (11)$$

This will modify the element stiffness matrix and the load vector. The relationship between blade pitch and pitch link displacement w_p is calculated iteratively.

The assembly of n elements yields the equation of motion in terms of nodal displacements $\{q\}$ as

$$[M(q)]\{\ddot{q}\} + [C(q)]\{\dot{q}\} + [K(q)]\{q\} = \{Q\} \qquad (12)$$

These are nonlinear equations in q. The next step is to apply geometric boundary conditions. For the torque tube end, the axial and lead-lag displacements are freely permitted and the pitch link joint is pin-ended. Therefore, there is no geometric constraints for the torque tube. On the other hand, the flexbeam is cantilevered at the hub and therefore the displacements u, v, v', w, w', and ϕ are all zero at the root of the flexbeam. The boundary conditions are applied to the global equations (12) by canceling out the rows and columns corresponding to these constraint displacements.

Solution Procedure

The first step is to determine blade steady equilibrium position. For a known thrust level, the collective pitch is calculated. For this collective pitch, an approximate value of pitch link position w_p is determined. Now with a known w_p as a boundary condition, the blade steady deflected position is calculated from the nonlinear equations (12), after dropping time dependent terms.

The second step is to obtain the coupled natural vibration (rotating) characteristics of the blade about its steady equilibrium position. Then, the flutter solution is obtained by assuming vibratory motion to be small perturbation about equilibrium position. For this, the normal mode equations are obtained and an eigen analysis is made. The nature of the complex eigenvalues explains whether blade is stable or not.

Results and Discussion

Numerical results are calculated for bearingless blade configurations, consisting of single flexbeam with wrap-around type torque tube (as shown in Fig. 2). For calculations, the blade is discretized into seven elements; three elements for main blade, two elements for flexbeam and two elements for torque tube. The normal mode stability solution is calculated using six coupled rotating modes. For analysis, the flexbeam and the torque tube are modelled as individual beams. At the root end, the flexbeam is rigidly fixed, whereas for the torque tube there are no constraints on displacements except for a spring restraint in the pitch link direction. A limiting case of rigid pitch link will result in complete displacement constraint at the pitch link location.

First, a correlation study of analytical results with the experimental data is attempted for selected bearingless blade configurations with conventional airfoil characteristics. The experimental stability data for a model rotor is taken from Ref. 6. The model rotor characteristics are Lock number $\gamma = 5.9$, solidity ratio $\sigma = 0.03$, three-bladed, and zero precone. The airfoil characteristics used are:

$$C_\ell = 0.15 + 5.73\alpha$$

$$C_d = 0.0079 + 1.79\alpha^2$$

$$C_m = -0.012$$

The idealized nondimensional structural properties used for elements are given in Table 1. Three different bearingless rotor configurations are considered depending on the pitch link location. The pitch links are located at a distance of 0.085R in the radial direction from the rotation axis. Fig. 7 presents the lag mode stability results for case I, where the pitch link is located at the leading edge of the torque tube. This positioning of pitch link will cause a positive pitch-flap coupling (flap up causing nose down pitch). In the figure, the damping of the fundamental lag mode in the form of

real part of the eigenvalue is plotted for different collective pitch angles. For this lag mode, a structural damping idealized by an equivalent viscous damping ratio of 1% is used. Based on the experience of stability correlations of other authors, it appears that the present analytical results are in good agreement with the experimental results. Fig. 8 shows the lag mode stability results for case II, where the pitch link is located at the trailing edge of the torque tube. This will cause a negative pitch-flap coupling. In Fig. 9, the results are presented for case III, where one pitch link is located at the leading edge and the other at the trailing edge of the torque tube. This will not cause any pitch-flap coupling, but it will raise the torsional frequency of the blade. Again, the agreement of analytical results with the experimental data appears quite satisfactory. It is also noted here that the inclusion of dynamic inflow has only a slight influence on lag mode stability.

The subsequent results are obtained for bearingless CCR blade configurations. These results are calculated for a CCR blade with Lock number $\gamma = 7.2$, solidity ratio $\sigma = 0.13$, four bladed, and zero precone. For simple airfoil characteristics, the following analytical expressions are used:

$$C_\ell = 0.3 + 6.7\alpha + 16.1C_\mu^{.67}$$

$$C_d = 0.026 - 0.3C_\mu^{.67}$$

$$C_{m_{.5}} = 0.06 + 1.34\alpha - 0.644C_\mu^{.67}$$

and these are gross representations of the data in Ref. 7. For table aerodynamics, the airfoil characteristics of a typical CC airfoil with single trailing edge slot are used. The slot height to chord ratio is taken as 0.002 and the airfoil thickness to chord ratio is taken as 0.15. The chordwise offsets of the center of mass, the aerodynamic center, and the tension center from the elastic axis are considered to be zero, and the elastic axis is assumed to be at mid-chord position. The non-dimensional structural blade properties for different elements are given in Table 2. For stability results, the inherent structural damping is assumed to be zero for all modes. Results are calculated for the CCR bearingless configurations, case III only, for which the pitch links are located at the leading edge and the trailing edge of the torque tube.

Fig. 10 shows for trim solutions in hover, the blowing momentum coefficient at the blade tip plotted as a function of rotor thrust for several collective pitch angles. It is assumed that the blowing coefficient varies inverse to the square of the radial position ($C_\mu = C_{\mu_T}/\xi^2$). Results are calculated using simple expressions as well as airfoil tables. With airfoil tables, an iterative procedure based on Newton-Raphson method is used to calculate the trim solution. There is a considerable disparity between the two results. This is understandable since simple expressions are only gross representation of the airfoil characteristics below stall, whereas the table data covers the complete range of angle of attack and blowing coefficient.

Fig. 11 shows the damping ratio ζ for three modes with less damping as a function of thrust level for a case with zero collective pitch ($\theta_0 = 0$). These less damped modes happen to be fundamental lead-lag, fundamental torsion and second lead-lag modes. The other modes are more damped for this as well as for subsequent cases and hence are not plotted. These results are calculated using the airfoil tables. The negative value of damping represents the instability condition of a mode. The lag mode is stable at low thrust levels and becomes unstable at high thrust levels. The torsion mode and the second lag mode are moderately unstable. All three modes can be easily stabilized with the inclusion of small amount of structural damping in these modes. Most rotor designs inherently have enough structural damping to stabilize these levels of instability. A similar type of stability characteristics were observed in Ref. 4 for hingeless CCR blades with zero collective pitch. In Fig. 12, the stability results are shown for the same blade configurations using the simple analytical expressions presented previously for the airfoil characteristics. Though this approximation is quite gross as seen in the trim solution (Fig. 8), the stability results are quite reasonably predicted. The inclusion of dynamic inflow has a slight influence on lag mode stability, in fact, a destabilizing effect at high thrust levels.

Fig. 13 shows the stability results for a negative collective pitch of -10^0 using the table aerodynamics. For this pitch setting, one needs a larger amount of blowing to acheive certain thrust level. The fundamental lag mode becomes unstable at low thrust levels, and becomes quite stable at high thrust levels. In fact, at low thrust levels one needs a larger amount of damping to stabilize this mode. The effect of negative pitch on torsion and second lag mode is comparatively less, it stabilizes the torsion mode somewhat. The effect of positive collective setting on blade stability is shown in Fig. 14. For this pitch, one needs a small amount of blowing to achieve certain thrust level. Here, the fundamental lag mode gets very stabilized. The influence on the other two modes is again small.

Conclusions

The aeroelastic stability of a bearingless circulation control rotor blade in hover is examined using a finite element formulation. Airfoil characteristics are represented in the form of simple expressions as well as in the form of data tables. The flexbeam, the torque tube and the main blade are modeled individually as elastic beams. Numerical results are calculated for a circulation control bearingless rotor configuration consisting of a single flexbeam with a wrap-around type torque tube and the pitch links located at both the leading edge and the trailing edge of the torque tube.

Based on this effort the following conclusions can be drawn:

(1) A reasonable correlation of analytical results with the experimental data for selected bearingless configurations with conventional airfoils has introduced confidence to the methodology and the algorithms.

(2) For flutter solution, one needs to include at least four modes; these are fundamental flap, lag, and torsion modes and the second lag mode.

(3) Stability results have shown that the trailing edge blowing plays an important role in the determination of the aeroelastic stability of a rotor blade.

(4) The inclusion of dynamic inflow has a slight influence on lag mode stability.

(5) The negative pitch setting destabilizes lag mode, in particular, at low thrust levels.

(6) The positive pitch setting stabilizes lag mode.

(7) For a fixed thrust level, it appears that going to higher blowing is more destabilizing.

(8) The fundamental torsion and the second lag modes are weakly unstable for some thrust levels. The expected levels of internal structural damping appear adequate to stabilize these modes.

ACKNOWLEDGEMENTS

The author wishes to acknowledge helpful discussions with Kenneth Reader, James Biggers, and Al Schwartz of David W. Taylor Naval Ship Research and Development Center. The work was supported by DTNSRDC under contract no. N-00167-84-M-1548. Acknowledgements are also due t U.S. Army Aeromechanics Laboratory, Ames Research Center for providing the rotor model data.

References

1. Ormiston, R.A., "Investigation of Hingeless Rotor Stability", Vertica, Vol. 7, No. 2, 1983, pp. 143-181.

2. Friedmann, P., "Formulation and Solution of Rotary-Wing Aeroelastic Stability and Response Problems", Vertica, Vol. 7, No. 2, 1983, pp. 101-141.

3. Chopra, I. and Johnson, W., "Flap-lag-torsion Aeroelastic Stability of Circulation-controlled Rotors in Hover", Journal of the American Helicopter Society, Vol. 24, No. 2, April 1979, pp. 37-46.

4. Chopra, I., "Aeroleastic Stability of an Elastic Circulation Control Rotor Blade in Hover", Appearing in Vertica, 1984.

5. Sivaneri, N.T. and Chopra, I., "Finite Element Analysis for Bearingless Rotor Blade Aeroelasticity", Journal of the American Helicopter Society, Vol. 29, No. 2, April 1984, pp. 42-51.

6. Dawson, S., "An Experimental Investigation on the Stability of a Bearingless Model Rotor in Hover," Journal of the American Helicopter Society, Vol. 28, No. 4, Oct. 1983, pp. 29-34.

7. William, R.M., Rogers, E.O. and Leitner, R.T., "X-Wing Technology Summary, Vol. II," DTNSRDC Report TM-16-76-72, June 1976.

Table 1. Structural properties of elements for rotation speed of 1100 RPM.

Element	Length ℓ/R	Flapwise $EI_y/m_o\omega^2R^4$	Chordwise $EI_z/m_o\Omega^2R^4$	Torsion $GJ/m_o\Omega^2R^4$	Mass m/m_o	Torsion inertia K_m^2/R^2	
1	0.367	0.0055	0.1501	0.0029	1.0	0.00091	Blade
2	0.367	0.0055	0.1501	0.0029	1.0	0.00091	Blade
3	0.069	0.1216	0.1216	0.2433	39.6	0.0105	Blade
4	0.113	0.00158	0.0052	0.00021	0.299	0.000029	Flex beam
5	0.085	2.099	2.099	9.150	72.6	0.0346	Flex beam
6	0.0564	4.257	4.257	1.815	7.63	0.0020	Torque tube
7	0.0564	4.257	4.257	1.815	7.63	0.0020	Torque tube

Chord/radius = .0465

Pitch link spring $\frac{K_p}{m_o\Omega^2R}$ = 171.06

Pitch link offset from torque tube center $\frac{d}{R}$ = .0409

$\eta_t = \eta_f = 0$

Table 2. Structural properties of elements for the circulation control bearingless blade.

Element	Length ℓ/R	Flapwise $EI_y/m_o\omega^2R^4$	Chordwise $EI_z/m_o\Omega^2R^4$	Torsion $GJ/m_o\Omega^2R^4$	Mass m/m_o	Torsion inertia K_m^2/R^2	
1	0.2	0.0186	0.2303	0.0297	0.7067	0.000739	Blade
2	0.2	0.0372	0.3938	0.0557	1.0	0.000832	Blade
3	0.2	0.0929	0.7133	0.0929	1.624	0.001068	Blade
4	0.2	0.1858	0.2303	0.00297	1.383	0.000099	Flexbeam
5	0.2	0.5573	0.6687	0.00297	1.556	0.000279	Flexbeam
6	0.13	0.0817	0.5201	0.1560	1.398	0.001397	Torque tube
7	0.13	0.1486	0.3901	0.2823	1.549	0.001366	Torque tube

Chord/radius = .1034

Pitch link spring $\frac{K_p}{m_o\Omega^2R}$ = 10000

Pitch link offset from torque tube center $\frac{d}{R}$ = .033

$\eta_t = \eta_f = 0$

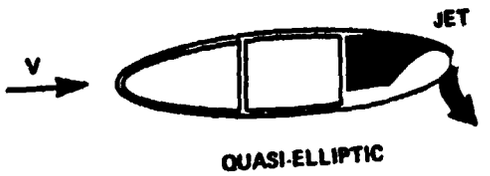

Fig. 1 Circulation control airfoil.

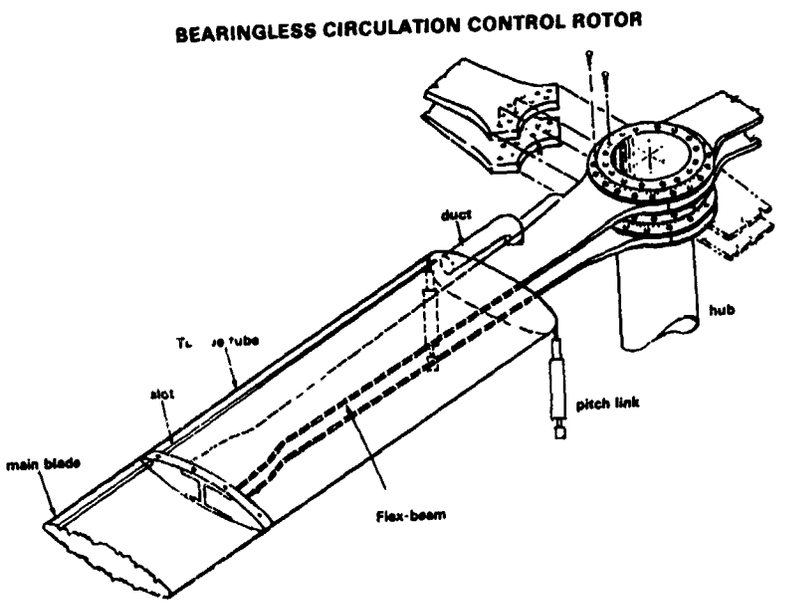

Fig. 2

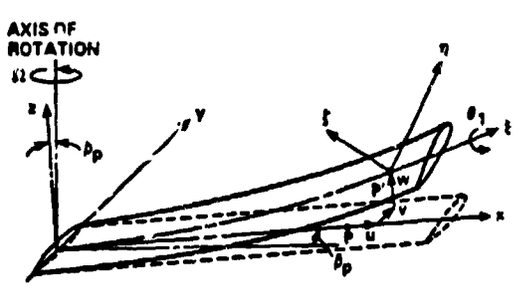

Fig. 3 Blade coordinate systems and deflections.

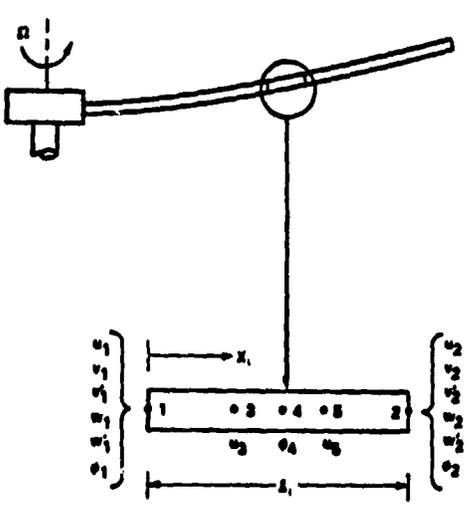

Fig. 4 A finite element showing nodal degrees of freedom.

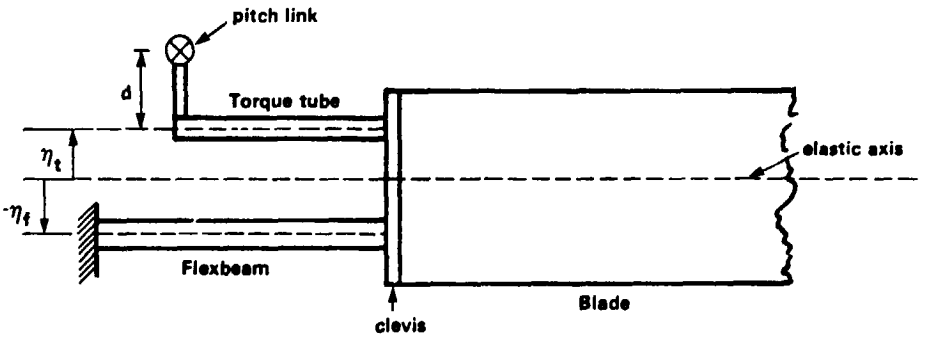

Fig. 5 Analytical model of a bearingless blade.

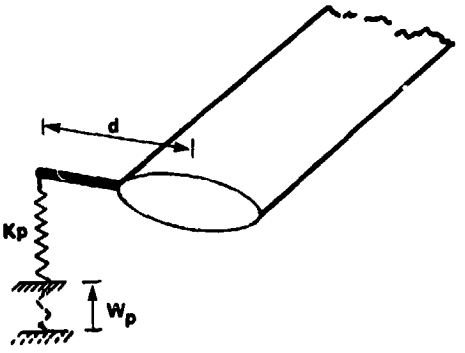

Fig. 6 Torque tube and pitch link.

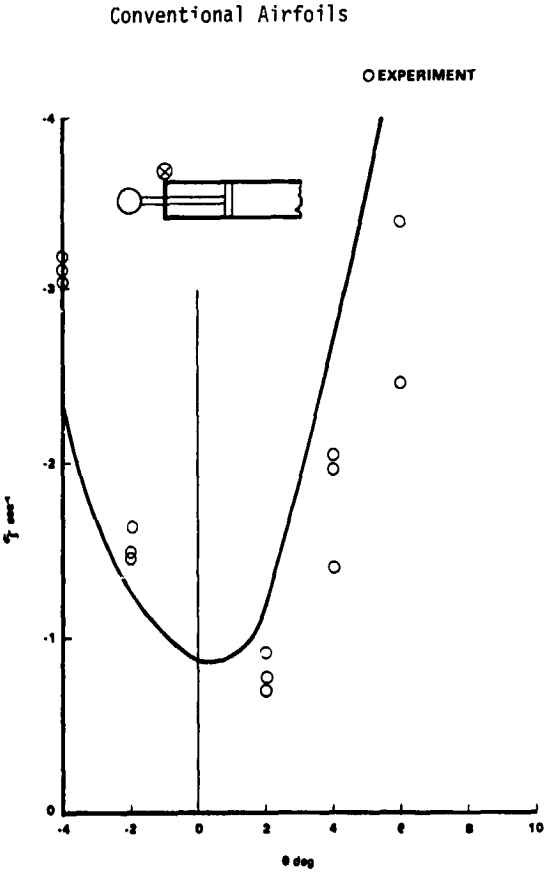

Fig. 7 Lag damping as a function of blade collective pitch, case I (pitch link at leading edge of torque tube).

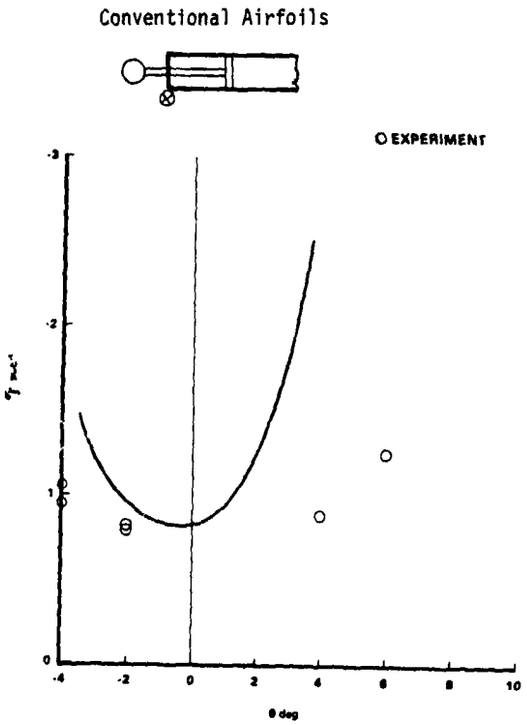

Fig. 8 Lag damping as a function of blade collective pitch, case II (pitch link at trailing edge of torque tube)

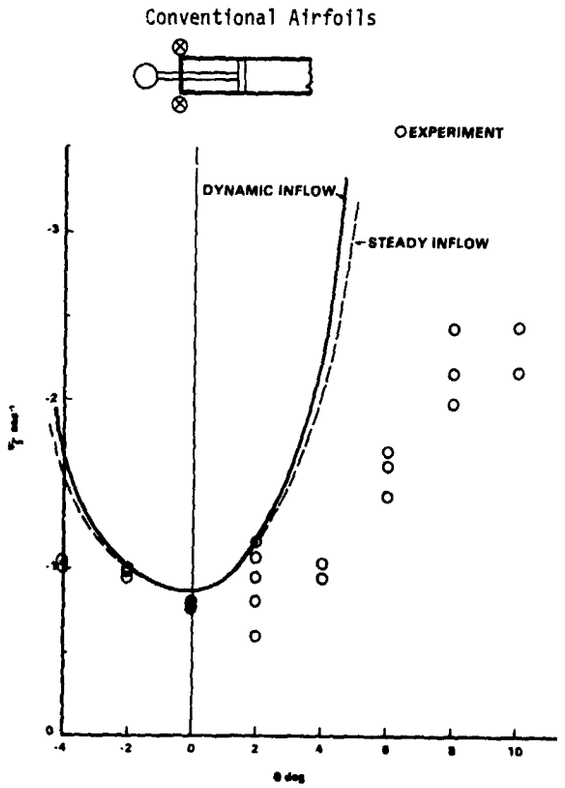

Fig. 9 Lag damping as a function of blade collective pitch, case III (pitch links at leading edge and trailing edge of torque tube).

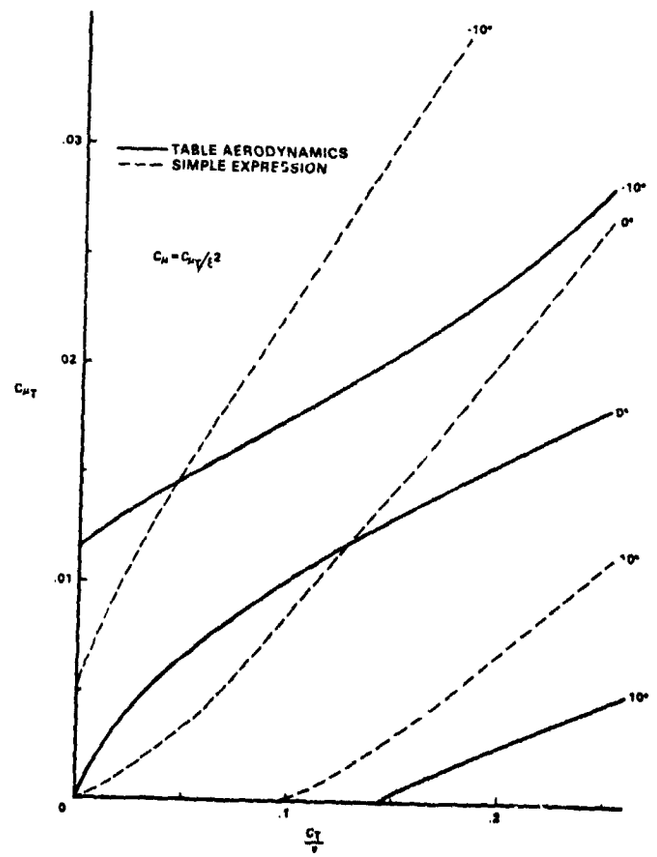

Fig. 10 Blade blowing coefficient as a function of rotor thrust and collective pitch.

CC Airfoils, $C_\mu = C_{\mu_T}/\xi^2$, Table Aerodynamics $\theta_o = 0$

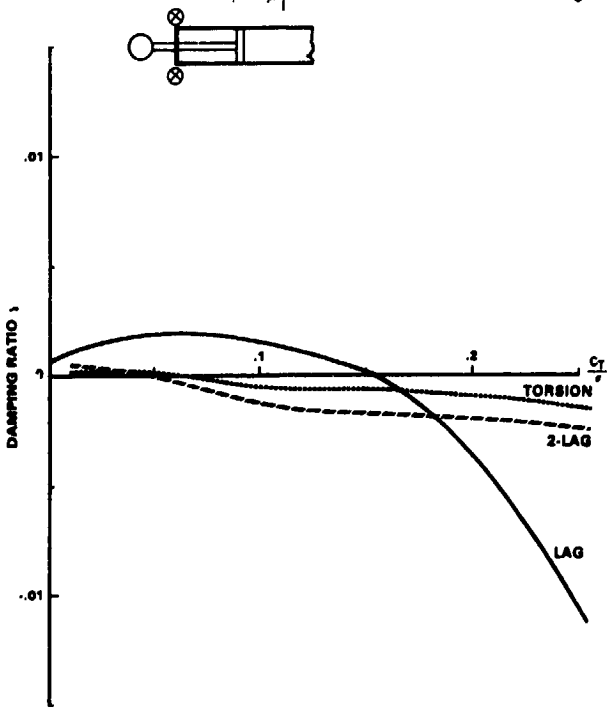

Fig. 11 Damping ratio for zero collective pitch (zero structural dampings, ω_v=2.5, ω_w=2.3, ω_ϕ=17.4)

CC Airfoils, $C_\mu = C_{\mu_T}/\xi^2$, Table Aerodynamics θ_o=-10°

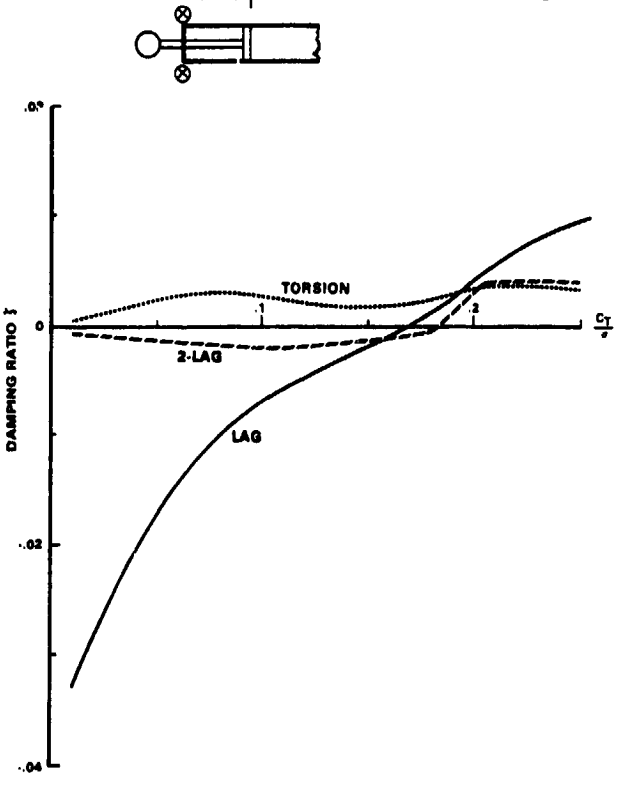

Fig. 13 Damping ratio for negative collective pitch (zero structural dampings, ω_v=2.5, ω_w=2.3, ω_ϕ=17.0)

CC Airfoils, $C_\mu = C_{\mu_T}/\xi^2$, Analytical Aerodynamics, θ_o=0

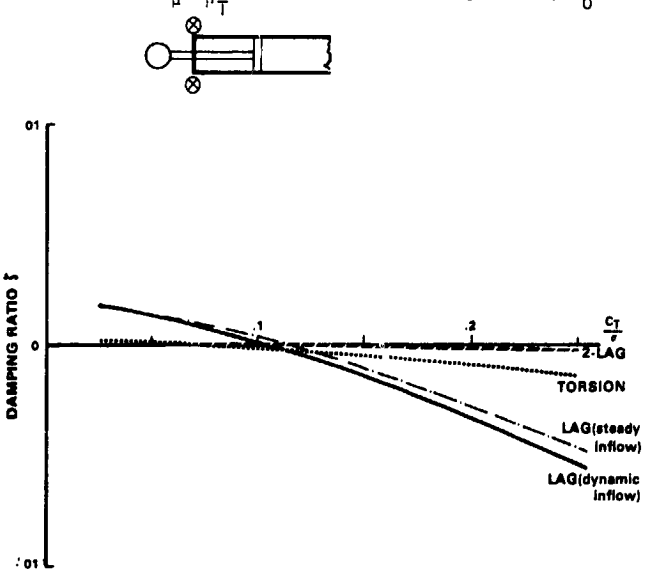

Fig. 12 Damping ratio for zero collective pitch (zero structural dampings, ω_v=2.5, ω_w=2.3, ω_ϕ=17.4)

CC Airfoils, $C_\mu = C_{\mu_T}/\xi^2$, Table Aerodynamics θ_o=10°

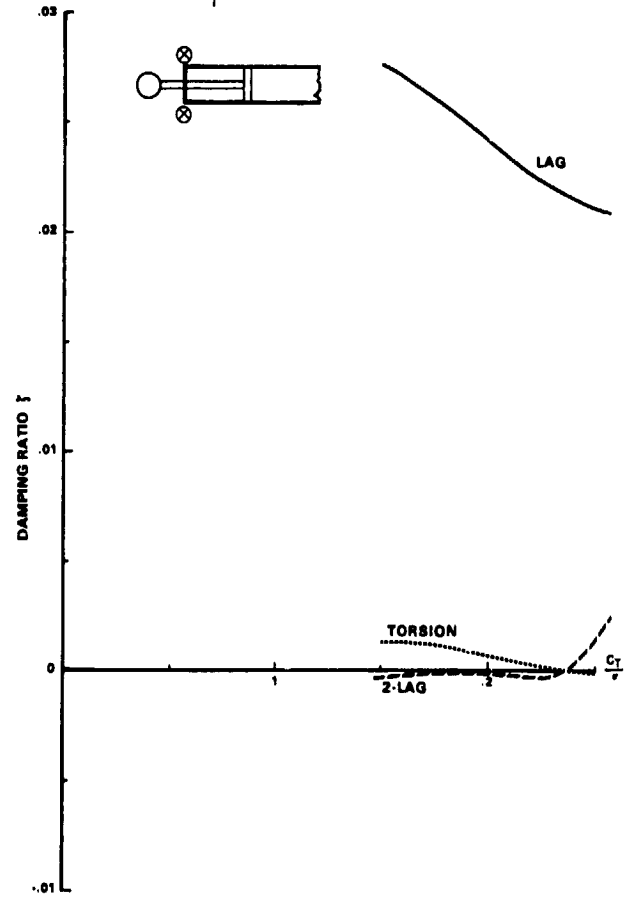

Fig. 14 Damping ratio for positive collective pitch (zero structural dampings, ω_v=2.5, ω_w=2.3, ω_ϕ=17.4)

DISCUSSION
Paper No. 17

DYNAMIC STABILITY OF A BEARINGLESS CIRCULATION CONTROL ROTOR BLADE IN HOVER
Inderjit Chopra

Jack Nielsen, NASA Ames Research Center: I have a serious question with regard to the fundamental aerodynamics of the problem. You have assumed you can calculate the flutter using steady aerodynamic results. Now we have a boundary layer on the Coanda plate and it isn't clear at all that at the frequencies of flutter that the boundary layer isn't going to have very important unsteady effects; we really don't know. But I don't think we can assume the quasisteady assumption offhand. Letting the amplitudes get small doesn't get around this problem if the unsteady effects are coupled into the flutter. So I would be interested to know since we don't have any data how you can be sure that you have really solved the real flutter problem for the CC airfoil.

Chopra: Are you posing the question [to me]? I do recognize that the unsteady aerodynamics for CCR is very important and it's not there. This is something that has to be looked at in the future. I am very much interested [and would] like to work on that problem if you give us the money.

Bill Warmbrodt, NASA Ames Research Center: The results that you showed for the circulation controlled airfoil showed damping ratios that were an order of magnitude lower than the hingeless configuration that you first showed the results for. You made mention that structural damping, had it been included, would have stabilized some of those modes. I think everybody in the audience here has a pretty good feel for what the influence of structural damping is for a hingeless rotor configuration. Would you say that you saw that same degree of sensitivity for the bearingless configurations that you analyzed?

Chopra: I think your first question is . . . let's look at it this way. You get lower damping here than you see in the hingeless [rotor]. I think that [you] have to go back and look first at the perturbation aerodynamics. Keep in mind that you are keeping your elastic axis at the half chord. Your perturbation aerodynamics has two components--[one] due to blowing, [one] due to conventional. The conventional part of the aerodynamics still has the quarter chord as the aerodynamic center and that will be destabilizing particularly for the torsion mode. So you expect to see lower damping. [This] means the people who have to design the X-Wing/CCR Rotor, they do need to--what should I say--add more structural damping or some sort of damping to stabilize these modes. I hope you may be agreeable to this point.

Jing Yen, Bell Helicopter: I understand that you used the normal modes approach to solve the problem. Would you like to tell us where and how you obtained the normal modes for the redundant or multiple load path hub? Also how much confidence [do] you have in [the modes]?

Chopra: The confidence is 100%. This is something [that is] a routine classroom problem. What we do is we look at first to the steady deflected shape and at that stage we solve the global equations. Solving the global [algebraic, eigenvalue] equation is very routine these days. It doesn't take any extra time. But when you are trying to solve the complex eigenvalue problem it is no good to use, say, a 100 by 100 equation, but it is good to use a 6 by 6 equation. There are two reasons for that--one is the computer and the second is the physical. You don't want to look at a hundred eigenvalues, you want to look at just five or six and see what is happening to [the major] mode shapes. Reducing to normal modes is the same [as] if you had got the mode shapes using the Myklestad method and reduce them to normal modes. I don't see any difference from the . . . if you were to [model] a beam [using], say, the Myklestad approach and 20 elements, you may be using only four or five modes. So the procedure is just the same. Did I satisfy?

Yen: This was a finite element model?

Chopra: It's a finite element model, yes. To start with it's a finite element model. We get the natural mode shape of [the blade] using finite elements. Redundancy doesn't come into the picture anywhere. This is only the way you are arranging the equations.

Peretz Friedmann: I think I misunderstood his question because I had the same concern about the redundancy. I think that when you have a redundant structure which is what [Jing] Yen alluded to you don't know exactly what the boundary conditions are and you might get incorrect mode shapes if you are not careful about the boundary conditions. I am not sure what those boundary conditions are because you have the cuff and you have the redundant load path and you really don't know what exactly the boundary condition is at the root. I think that's what he meant.

Chopra: I think that [is true with] any problem. If we don't know the boundary conditions we can make an error in any analysis. Some of the configurations I've seen, the pitch links seem to be . . . you can easily [get] the moment there and the only really important displacement is

the vertical displacement. But we did make a parametric study where we tried to constrain the pitch link. We tried to put various types of constraints on the pitch link. It is not very sensitive on stability.

Wayne Johnson: Aren't your normal modes, though, calculated after you find the deflected solution using the full finite element.

Chopra: That's right.

Johnson: So the normal modes are found after you have identified the boundary conditions.

Chopra: That's right, after identifying the boundary conditions, that's right.

Johnson: I think modes in this case is simply a way to reduce the dimension of the state vector. I don't think it really does anything more than that.